H1prelim-09-014 Submitted to

XVII International Workshop on Deep Inelastic Scattering, DIS2009, April 26-30, 2009, Madrid
Parallel Session **Diffraction and vector mesons**

Electronic Access: www-h1.desy.de/publications/H1preliminary.short_list.html

Deeply Virtual Compton Scattering and its Beam Charge Asymmetry in ep Collisions at HERA

H1 Collaboration

Abstract

A measurement of elastic deeply virtual Compton scattering $\gamma^* p \to \gamma p$ using the complete set of e^+p and e^-p collision data recorded with the H1 detector at HERA since 2003 is presented. The analysed data sample corresponds to an integrated luminosity of 306 pb^{-1}, almost equally shared between both beam charges. The cross section is measured as a function of the virtuality Q^2 of the exchanged photon and the centre–of–mass energy W of the $\gamma^* p$ system in the kinematic domain $6.5 < Q^2 < 80$ GeV^2, $30 < W < 140$ GeV and $|t| < 1$ GeV^2, where t denotes the squared momentum transfer at the proton vertex. The cross section is determined differentially in t for different Q^2 and W values and exponential t–slope parameters are derived. Using e^+p and e^-p data samples, a beam charge asymmetry is extracted for the first time in the low $x \simeq Q^2/W^2$ kinematic domain. The observed asymmetry is attributed to the interference between Bethe–Heitler and deeply virtual Compton scattering (DVCS) processes. This interference term is sensitive to the real part of the DVCS amplitude. The ratio of real to imaginary parts of the DVCS amplitude is then derived and is interpreted using dispersion relations. Experimental results are discussed in the context of two different models, one based on Generalised Parton Distributions (GPDs) and another on the dipole approach.

1 Introduction

Two main approaches govern the exploration of the microscopic structure of matter. First, the spatial distribution of matter, or charge, in a system can be probed through elastic scattering of electrons or photons. The measured physical quantities are the elastic form factors which depend on the four–momentum transfer to the system. The Fourier transformation of the form factors directly provides information on the spatial distribution of charges in the Breit frame. The second approach is designed to measure the momentum distribution, through deep inelastic scattering (DIS). Both approaches are complementary and suffer different drawbacks. The form factor measurements do not yield any information about the underlying dynamics of the system such as the momenta of the constituents, whereas the momentum distribution does not give any information on the spatial location of the constituents. In fact, more complete information about the microscopic structure lies in the correlation between momenta. This is an important issue for modern lepton–nucleon scattering experiments which aspire to measure the spatial distribution of quarks and gluons in the proton at the femtometer scale [1–7]. New results in this direction are presented in this paper.

Hard exclusive particle production, without excitation or dissociation of the nucleon, have emerged in recent years as prime candidates to address these issues. Among them, deeply virtual Compton scattering (DVCS) on the proton ($\gamma^* p \to \gamma p$), is the simplest. The DVCS reaction can be regarded as the elastic scattering of the virtual photon off the proton via a colourless exchange, producing a real photon in the final state. In the Bjorken scaling regime (large Q^2 and $|t|/Q^2 \ll 1$), QCD calculations assume that the exchange involves two partons in a colourless configuration, having different longitudinal and transverse momenta. These unequal momenta, or skewing, are a consequence of the mass difference between the incoming virtual photon and the outgoing real photon and may be interpreted in the context of Generalised Parton distributions (GPDs) and dipole amplitudes, respectively. In basic terms, a GPD (off–diagonal parton distribution) is then the quantum amplitude for removing a parton from the fast moving nucleon (proton in our case) and putting it back with a different momentum, thereby imparting a certain momentum transfer to the nucleon. The t–dependence of the DVCS cross section carries information on the transverse momentum of partons, which is also incorporated in GPDs or dipole amplitudes.

In the kinematic range of the HERA collider, as for all exclusive processes, the DVCS amplitude is mainly imaginary, while the change of the amplitude with energy gives rise to a small real part. To measure directly the real part of the amplitude, an interference between the exclusive process and a reference real scattering amplitude is needed. This is the case for the DVCS process, which interferes with the Bethe–Heitler (BH) process, but not for other exclusive processes like the production of vector mesons at HERA. In addition, the real part of the DVCS amplitude can be related to its imaginary part using dispersion relations. These relations are based on the analyticity of the amplitude and were first applied to proton–proton scattering in 1964 [8]. In the high energy limit at low x, they take a simple form [9] which can therefore be used for the DVCS process to verify the consistency between measurements of the real and imaginary parts of the amplitude.

This paper presents a new measurement of single and double differential DVCS cross sections as a function of the virtuality Q^2 of the exchanged photon and the $\gamma^* p$ centre–of–mass energy W. The single differential cross section $d\sigma/dt$ is also extracted. The data were recorded in the years 2003 to 2007 with the H1 detector when HERA collided protons of 920 GeV energy with 27.6 GeV electrons and positrons. The total integrated luminosity of the data is 306 pb^{-1}. The data comprise 162 pb^{-1} recorded in e^+p and 144 pb^{-1} in e^-p collisions. During the HERA II running period, the electron beam was longitudinally polarised, at a level of typically 35%. For this analysis, the periods with left–handed and right–handed beams are combined and the analysed data samples have a left–handed residual polarisation of 1% and 5% for e^+p and e^-p collisions, respectively. Cross section measurements are carried out in the kinematic range $6.5 < Q^2 < 80$ GeV^2, $30 < W < 140$ GeV and $|t| < 1$ GeV^2. The range in x of the present measurement extends from $5\ 10^{-4}$ to 10^{-2}. With a doubling of the integrated luminosity, this analysis supersedes cross section measurements from a previous H1 publication [10]. In addition, using both beam charges, the beam charge asymmetry (BCA) of the interference between the BH and DVCS processes is measured for the first time at a collider. From this asymmetry, the ratio of real to imaginary parts of the DVCS process is obtained.

In this paper, cross section measurements are compared to predictions based on GPDs or a dipole approach. At the present level of understanding, the pure GPDs approach and dipole models, based on the proton–dipole amplitude, are not connected. However, in the low x domain, dipole amplitudes could be used to provide parametrisations for GPDs at a certain scale [11]. In this context, the DVCS process is interesting as calculations are simplified by the absence of complications arising from an unknown vector meson wave function. DVCS is then the most interesting reaction to discuss models and provide further insights into GPDs or dipole amplitudes. The comparisons presented in this paper for both models are a first step in studying their consistency. The GPDs model [6] used has been shown to be accurate by previous data. It is based on partial wave expansions of DVCS amplitudes and is a first attempt to parametrise all GPDs over the full kinematic domain. The dipole approach [12] is very efficient at describing low x measurements at HERA, from inclusive to exclusive processes. In this model, mainly based on the gluon density extracted from fits to F_2 data, the DVCS cross section is computed using a universal dipole amplitude. Some additional terms enter the amplitude to take into account genuine saturation effects at the amplitude level [12].

For GPDs models, a direct measurement of the real part of the DVCS amplitude is an important issue, as it gives an increased sensitivity to the parametrisation of the GPDs [2, 6]. Indeed, a calculation of the real part of the DVCS amplitude needs a parametrisation of the GPDs over the full x range. Therefore, the prediction of this quantity is a challenge for models. Conversely, different GPDs models can be validated or rejected on the basis of measurements of the real part of the amplitude. Considering the large flexibility in GPDs parametrisation, this is an important quantity to qualify the correct approaches of GPDs [2, 6]. In the dipole approach, as the dipole amplitude refers only to the imaginary part, the magnitude of the real part can be estimated using a dispersion relation.

2 DVCS, Beam Charge Asymmetry and Dispersion Relations

In high energy electron–proton collisions at HERA, DVCS is accessed through the reaction $e^{\pm}p \to e^{\pm}\gamma p$ [10, 13–16]. This reaction also receives a contribution from the purely electromagnetic BH process, where the photon is emitted from the electron. The BH cross section is precisely calculable in QED and can be subtracted from the total process rate to extract the DVCS cross section.

Since these two processes have an identical final state, they can interfere. The squared photon production amplitude is then given by

$$|A|^2 = |A_{BH}|^2 + |A_{DVCS}|^2 + \underbrace{A_{DVCS}\, A^*_{BH} + A^*_{DVCS}\, A_{BH}}_{I}, \tag{1}$$

where A_{BH} is the real BH amplitude, A_{DVCS} represents the DVCS amplitude and I denotes the interference term. In the leading twist approximation, the interference term can be written quite generally as a linear combination of harmonics of the azimuthal angle ϕ. As defined in [2], ϕ is the angle between the plane containing the incoming and outgoing leptons and the plane formed by the virtual and real photons. If only the first term in $\cos\phi$ and $\sin\phi$ are considered and for an unpolarised proton beam, the interference term I can be written as

$$I \propto -C\,[a\cos\phi\,\mathrm{Re}A_{DVCS} + bP_l\sin\phi\,\mathrm{Im}A_{DVCS}], \tag{2}$$

where $C = \pm 1$ is the charge of the lepton beam, P_l its longitudinal polarisation and a and b are functions of the ratio of longitudinal to transverse virtual photon flux [1–6]. Cross section measurements which are integrated over ϕ are not sensitive to the interference term, but the measurement of a cross section asymmetry with respect to the beam charge allows its extraction. The cross section asymmetry is expressed as

$$A_C = \frac{d\sigma^+/d\phi - d\sigma^-/d\phi}{d\sigma^+/d\phi + d\sigma^-/d\phi}, \tag{3}$$

where $d\sigma^+/d\phi$ and $d\sigma^-/d\phi$ are the DVCS cross sections measured in e^+p and e^-p collisions, respectively. If the contribution from the polarisation effect in $\sin\phi$ is neglected and only the first term in $\cos\phi$ is considered, A_C can be expressed as

$$A_C = p_1\cos\phi = 2A_{BH}\frac{\mathrm{Re}A_{DVCS}}{|A_{DVCS}|^2 + |A_{BH}|^2}\cos\phi. \tag{4}$$

The term $|A_{DVCS}|^2$ can be derived directly from the DVCS cross section measurement. As the BH amplitude is precisely known, the measured asymmetry is directly proportional to the real part of the DVCS amplitude.

The value of the ratio between real and imaginary parts of the DVCS amplitude, $\rho = \mathrm{Re}A_{DVCS}/\mathrm{Im}A_{DVCS}$, can be extracted using equation (4) and the expression for the imaginary part of the DVCS amplitude

$$\mathrm{Im}A_{DVCS} = \sqrt{\frac{|A_{DVCS}|^2}{1+\rho^2}}. \tag{5}$$

The ratio ρ can also be derived using a dispersion relation [6, 8, 17]. In the high energy limit, at low x and when the W dependence of the cross section is dominated by a single term in $W^{\delta(Q^2)}$ (with $\delta(Q^2) > 0.3$), the dispersion relation can be written as [9]

$$\rho = \mathrm{Re}A_{DVCS}/\mathrm{Im}A_{DVCS} = \tan\left(\frac{\pi\delta(Q^2)}{8}\right). \tag{6}$$

The ratio ρ can therefore be estimated directly from the energy dependence $\delta(Q^2)$ of the DVCS cross section. Comparison with the ρ value calculated from the energy dependence of the DVCS amplitude therefore provides an important consistency test of the measured BCA.

3 Experimental Conditions and Monte Carlo Simulation

A detailed description of the H1 detector can be found in [18]. Here, only the detector components relevant for the present analysis are described. H1 uses a right–handed coordinate system with the z axis along the beam direction, the $+z$ or "forward" direction being that of the outgoing proton beam. The polar angle θ is defined with respect to the z axis and the pseudo–rapidity is given by $\eta = -\ln\tan\theta/2$. The SpaCal [19], a lead scintillating fibre calorimeter, covers the backward region ($153° < \theta < 176°$). Its energy resolution for electromagnetic showers is $\sigma(E)/E \simeq 7.1\%/\sqrt{E/\mathrm{GeV}} \oplus 1\%$. The liquid argon (LAr) calorimeter ($4° \leq \theta \leq 154°$) is situated inside a solenoidal magnet. The energy resolution for electromagnetic showers is $\sigma(E)/E \simeq 11\%/\sqrt{E/\mathrm{GeV}}$ as obtained from test beam measurements [20]. The main component of the central tracking detector is the central jet chamber CJC ($20° < \theta < 160°$) which consists of two coaxial cylindrical drift chambers with wires parallel to the beam direction. The measurement of charged particle transverse momenta is performed in a magnetic field of 1.16 T, which is uniform over the full tracker volume. The innermost proportional chamber CIP ($9° < \theta < 171°$) is used in this analysis to complement the CJC in the backward region for the reconstruction of the interaction vertex. The forward muon detector (FMD) consists of a series of drift chambers covering the range $1.9 < \eta < 3.7$. Primary particles produced at larger η can be detected indirectly in the FMD if they undergo a secondary scattering with the beam pipe or other adjacent material. Therefore, the FMD is used in this analysis to provide an additional veto against inelastic or proton dissociative events. The luminosity is determined from the rate of Bethe–Heitler processes measured using a calorimeter located close to the beam pipe at $z = -103$ m in the backward direction.

A dedicated event trigger was set up for this analysis. It is based on topological and neural network algorithms and uses correlations between electromagnetic energy deposits of electrons or photons in both the LAr and the SpaCal [21]. The combined trigger efficiency is 98%.

Monte Carlo (MC) simulations are used to estimate the background contributions and the corrections that must be applied to the data to account for the finite acceptance and the resolution of the detectors. Elastic DVCS events in ep collisions are generated using the Monte Carlo generator MILOU [22], based on the cross section calculation from [23] and using a t–slope parameter $b = 5.4$ GeV^{-2}, as measured in this analysis (see section 6.1). Inelastic DVCS events in which the proton dissociates into a baryonic system Y are also simulated with MILOU setting the t–slope b_{pdiss} to 1.5 GeV^{-2}, as determined in a dedicated study (see section 6.2). The Monte Carlo program COMPTON 2.0 [24] is used to simulate elastic and inelastic BH events. In the generated MC events, no interference between DVCS and BH processes is included. The background source of diffractive meson events is simulated using the DIFFVM MC generator [25]. All generated events are passed through a detailed, GEANT [26] based, simulation of the H1 detector and are subject to the same reconstruction and analysis chain as the data.

4 Event Selection

In elastic DVCS events, the scattered electron and the photon are the only particles that should give signals in the detector. The scattered proton escapes undetected through the beam pipe. The selection of the analysis event sample requires the scattered electron to be detected in the SpaCal and the photon in the LAr. The energy of the scattered electron candidate must be greater than 15 GeV. The photon is required to have a transverse momentum P_T above 2 GeV and a polar angle between $25°$ and $145°$. Events are selected if there are either no tracks at all or a single central track which is associated with the scattered electron. In order to reject inelastic and proton dissociation events, no further energy deposit in the LAr calorimeter larger than 0.8 GeV is allowed and no activity above the noise level should be present in the FMD. The influence of QED radiative corrections is reduced by the requirement that the longitudinal momentum balance $E - P_z$ be greater than 45 GeV. Here, E denotes the energy and P_z the momentum along the beam axis of all measured final state particles. To enhance the DVCS signal with respect to the BH contribution and to ensure a large acceptance, the kinematic domain is restricted to $6.5 < Q^2 < 80$ GeV^2 and $30 < W < 140$ GeV.

The reconstruction method for the kinematic variables Q^2, x and W relies on the measured polar angles of the final state electron and photon (double angle method) [10]. The variable t is approximated by the negative square of the transverse momentum of the outgoing proton, computed from the vector sum of the transverse momenta of the final state photon and the scattered electron [10]. The resolution of the t reconstruction lies in the range 0.06 to 0.20 GeV^2, from small to large $|t|$ values.

The selected analysis event sample contains 2643 events in e^+p and 2794 events in e^-p collisions, respectively. The MC expectations of the different processes are also displayed. Each source is normalised to the data luminosity. A good description of the shape and normalisation of the measured distributions is observed. The analysis sample contains contributions from the elastic DVCS and BH processes, as well as backgrounds from the BH and DVCS processes with proton dissociation, $ep \rightarrow e\gamma Y$, where the baryonic system Y of mass M_Y is undetected. The total contribution of proton dissociation from DVCS and BH processes is found to be $14 \pm 4\%$, as estimated from MC predictions. Other backgrounds from diffractive ω and ϕ production with decay modes to final states including photons are estimated to be negligible in the kinematic range of the analysis. Background contribution from interactions in beam satellites is found to be below 1%, as estimated from the data. Contamination from processes with low multiplicity π^0 production was also investigated and found to be negligible.

5 Cross Section and Beam Charge Asymmetry Measurements

The DVCS and BH contributions are dominant in the analysis phase space. For a measurement integrated over the angle ϕ, the contribution of the interference term I is small (below 1%). The full $e^{\pm}p$ data sample can therefore be used to measure the DVCS cross section integrated over this angle. The separate e^+p and e^-p data samples are used to measure the amplitude of the interference term.

The DVCS cross section, $\gamma^* p \to \gamma p$, is evaluated in each bin i at the bin centre values Q_i^2, W_i, t_i, from the total number $N_i^{\rm obs}$ of data events in the analysis sample using the expression

$$\sigma_{DVCS}(Q_i^2, W_i, t_i) = \frac{(N_i^{\rm obs} - N_i^{\rm BH} - N_i^{\rm pdiss})}{N_i^{\rm DVCS}} \cdot \sigma^{\rm th}_{DVCS}(Q_i^2, W_i, t_i). \tag{7}$$

The other numbers in this equation are calculated using the MC simulations described in section 3. $N_i^{\rm BH}$ denotes the number of BH events (elastic and inelastic) reconstructed in bin i, $N_i^{\rm pdiss}$ the number of inelastic DVCS background events, $N_i^{\rm DVCS}$ the number of DVCS events computed from the elastic DVCS MC and $\sigma^{\rm th}_{DVCS}$ is the theoretical DVCS cross section used for the generation of DVCS MC events.

The mean value of the acceptance, defined as the number of MC events reconstructed in a bin divided by the number of events generated in the same bin, is 60% over the whole kinematic range, for both beam charges. The acceptance reaches 86% for the highest t bin. The systematic errors of the measured DVCS cross section are determined by repeating the analysis after applying to the MC appropriate variations for each systematic source. The main contribution comes from the acceptance correction factors calculated by varying the t–slope parameter set in the elastic DVCS MC by $\pm 6\%$, as constrained by this analysis. The uncertainty on the number of elastic DVCS events lost by the application of the FMD veto is modelled by a 4% variation of the FMD efficiency. Both error sources combined result in an error of 10% on the measured elastic DVCS cross section. The uncertainty related to the inelastic DVCS background is estimated from the variation of its t–slope parameter by 20% around the nominal value of $b_{pdiss} = 1.5$ GeV^{-2} (see section 6.2). The resulting error on the elastic DVCS cross section amounts to 4% on average and reaches 12% at high t. The contribution from BH processes is controlled using the method detailed in [10]. A systematic uncertainty of 3% is estimated for this contribution. The uncertainties related to subtraction of the BH background, trigger efficiency, photon identification efficiency, radiative corrections and luminosity measurement are each in the range of 1 to 3%. The total systematic uncertainty of the cross section amounts to about 12%, 85% of which are correlated errors.

For the BCA measurement, the angle ϕ is calculated from the reconstructed four–vectors of the electron and of the photon. Note that ϕ is not defined when $|t| < |t|_{min} \simeq x^2 m_p^2/(1-x) \sim 10^{-5}$, where m_p is the mass of the proton [2]. From MC studies, the resolution on ϕ is of the order of 20° to 40°, with large migrations between the true and the reconstructed $|\phi|$ from 0° to 180°, and vice versa. The resolution on ϕ is limited mainly by the resolution on the photon energy in the LAr and the resolution on the electron polar angle. The asymmetry A_C is then determined from the differential cross sections $d\sigma^+/d\phi$ and $d\sigma^-/d\phi$ using the formula (3). Events with $\phi < 0$ and $\phi > 0$ are combined, in order to increase the statistical significance and to remove effects on the asymmetry of any possible $\sin\phi$ contribution from the residual lepton beam polarisation. The systematic error on the BCA measurement mainly arises from the correlated part of the LAr photon energy scale uncertainty, which is estimated to be 0.5% between both e^+p and e^-p samples.

Due to the limited statistics and the large experimental resolution on ϕ, the data are not sensitive to further possible harmonics beyond a pure $\cos\phi$. In addition, from theoretical predictions, the first $\cos\phi$ harmonic is expected to be the dominant one. A generated asymmetry of the form $p_1\cos\phi$ is therefore added to the MC and passed through the full detector simulation and analysis chain to account for all acceptance and migration effects from true to reconstructed ϕ values. A χ^2 minimisation is then performed as a function of the parameter p_1 to adjust the reconstructed asymmetry to the measured one. The difference between the true and the reconstructed asymmetry is then used to determine bin by bin correction factors to account for the effect of migrations on the measured asymmetry.

6 Experimental Results and Interpretations

6.1 Cross Sections and t–dependence

The complete $e^{\pm}p$ DVCS sample is used to extract the W dependence of the DVCS cross section expressed at $Q^2 = 10$ GeV^2 as well as the Q^2 dependence at $W = 82$ GeV. The results are displayed in figure 1, and are in agreement within errors with the previous measurements [10, 14–16]. Experimental results are compared with a model based on GPDs [6] or a dipole approach [12]. A good agreement is observed in both cases. DVCS cross sections for both e^+p and e^-p data are also found to be in good agreement. As already discussed in [10], the steep rise of the cross section with W is an indication of the presence of a hard underlying process.

Next, the W dependence of the DVCS cross section is determined for three separate ranges of Q^2, as shown in figure 2(a). A fit of the form W^δ is performed to the cross section in each Q^2 range. Figure 2(b) presents the δ values obtained as a function of Q^2. It is observed that δ is independent of Q^2 within the errors. Using the complete analysis sample, the value of δ expressed at $Q^2 = 10$ GeV^2 is found to be $0.63 \pm 0.08 \pm 0.14$, where the first error is statistical and the second systematic. It is in agreement with the δ value previously measured in [10], as well as with the value of $\delta = 0.52 \pm 0.09$ (stat.) measured by the ZEUS Collaboration at a lower Q^2 of 3.2 GeV^2 [16].

Fits of the form $d\sigma/dt \sim e^{-b|t|}$ are performed taking into account the statistical and correlated systematic errors. The derived t–slope parameters $b(Q^2)$ and $b(W)$ are displayed in figures 3(a) and (b), respectively. It confirms the result obtained in a previous analysis [10] and no significant variation of b with W is observed. Again, experimental results are compared with predictions from GPDs and dipole models [6,12]. A good agreement is obtained for both W and Q^2 dependences of the t–slopes. If b is parametrised as $b = b_0 + 2\alpha' \ln\frac{1}{x}$, an upper limit on α' of 0.20 GeV^{-2} at 95% confidence level (CL) is derived. This value, in the Q^2 range of the present analysis, is compatible with results obtained for J/ψ exclusive electroproduction [27, 28], for which the measured α' is below 0.17 GeV^{-2} at 95% CL. Shrinkage is therefore not observed and equally, at the presently available W values, Gribov diffusion [29] is unimportant in this process and the average k_T exchanged during the reaction remains large. Such a behaviour is expected for hard processes and confirms that perturbative QCD can be used to describe DVCS processes.

Using the complete analysis sample, the value of b expressed at $Q^2 = 10$ GeV^2 is found to be $5.41 \pm 0.14 \pm 0.31$ GeV^{-2}, where the first error is statistical and the second systematic. It corresponds to a total uncertainty of 6% on the (elastic) t–slope measurement for the full data sample. As in [10], this t–slope value can be converted to an average impact parameter of $\sqrt{< r_T^2 >} = 0.64 \pm 0.02$ fm. It corresponds to the transverse extension of the parton density, dominated by sea quarks and gluons for an average value $x = 1.2\ 10^{-3}$, in the plane perpendicular to the direction of motion of the proton. At larger values of x ($x > 0.1$), a smaller value of $\sqrt{< r_T^2 >}$, dominated by the contribution of valence quarks, is expected. In this kinematic domain, only indirect determinations exist [7]. From these indirect determinations, the evolution of $\sqrt{< r_T^2 >}$ as a function of x can be estimated. For $x < 0.01$, as measured in this paper, the average transverse size is 0.64 fm and it reaches 0.4 fm for $x > 0.2$ [4]. This gives the two dimensional density profile of partons in the proton.

6.2 Inelastic DVCS t–dependence

The increased statistic compared to previous analyses allowed a first measurement of the t–slope of the inelastic DVCS process. A sample of events with a signal in the FMD is selected. It corresponds, from MC studies, to events with the mass of the proton dissociation system $M_Y > 1.4$ GeV. The contribution of inelastic DVCS events is extracted by subtracting the BH and elastic DVCS contributions, as estimated from the respective MC expectations. The measured differential cross section as a function of t are presented in figure 4. A fit of the form $d\sigma/dt \sim e^{-b_{pdiss}|t|}$ yields $b_{pdiss} = 1.53 \pm 0.26 \pm 0.44$, where the first error is statistical and the second systematic. This value is compatible with previous determinations for inelastic exclusive production of ρ, ϕ [30,31] and J/Ψ [32]. No indication of a dependence of b_{pdiss} with Q^2 or W is observed.

6.3 Beam Charge Asymmetry

The equal contributions of elastic DVCS and BH processes to the analysis sample provide a very favourable situation for the beam charge asymmetry measurement, with a maximum contrast for the interference term. The measured BCA integrated over the kinematic range of the analysis and corrected from detector effects, as detailed in section 5, is presented in figure 5. The χ^2 minimisation procedure leads to a p_1 value of $p_1 = 0.16 \pm 0.04 \pm 0.06$, where the first error is statistical and the second systematic. The function $0.16 \cos\phi$ is represented in figure 5 and is compared to the prediction of the GPDs model for the first $\cos\phi$ harmonic [6]. The measured asymmetry is in good agreement with the model prediction within experimental errors.

As detailed in section 2, from the measured BCA and the p_1 value determined above, together with the DVCS cross section, the ratio ρ of the real to imaginary parts of the DVCS amplitude can be calculated as

$$\rho = 0.20 \pm 0.05 \pm 0.08, \tag{8}$$

where the first error is statistical and the second systematic. This is a first direct determination of this ratio, made possible by the BCA measurement.

As discussed in section 2, the ratio $\rho = \mathrm{Re}A_{DVCS}/\mathrm{Im}A_{DVCS}$ can also be extracted using the dispersion relation of equation (6), leading to

$$\rho = 0.25 \pm 0.03 \pm 0.05, \tag{9}$$

where the first error is statistical and the second systematic. Both results (8) and (9) are in good agreement, which confirms the measurement of the real part of the DVCS amplitude from the BCA.

In the low x domain of the present measurement, the real part of the DVCS amplitude is therefore positive. In contrast, at larger x ($x \sim 0.1$) and lower Q^2, a smaller and negative real part was measured by the HERMES Collaboration [33, 34]. This result obtained by HERMES in a different x domain does not correspond to a hard energy dependence. In order to analyse the transition region from the x range of our measurements, $x < 0.01$, to the HERMES domain, $x \sim 0.1$, the future program of COMPASS will be important [35]. It could provide a measurement of the DVCS cross section in exactly the right, intermediate x domain to allow a detailed study of the transition region.

7 Conclusion

The cross section DVCS $\gamma^* p \to \gamma p$ has been measured with the H1 detector at HERA. The measurement is performed in the kinematic range $6.5 < Q^2 < 80$ GeV^2, $30 < W < 140$ GeV and $|t| < 1$ GeV^2. The analysis uses e^+p and e^-p data recorded from 2003 to 2007, corresponding to a total integrated luminosity of 306 pb^{-1}, almost equally shared between both beam charges. The W dependence of the DVCS cross section is well described by a function W^δ. No significant variation of the exponent δ as a function of Q^2 is observed. For the total sample a value $\delta = 0.63 \pm 0.08 \pm 0.14$ is determined. The steep rise of the cross section with W indicates a hard underlying process. The t–dependence of the cross section is well described by the form $e^{-b|t|}$ with an average slope of $b = 5.41 \pm 0.14 \pm 0.31$ GeV^{-2}. The t–slopes are determined differentially in W with no significant dependence observed, which confirms previous results. The study of the Q^2 dependence of b is found to be in good agreement with a slow decrease of b as a function of Q^2, compatible with previous observations. The measured DVCS cross section is compared to the predictions of two different models based on GPDs or on a dipole approach, respectively. Both approaches describe the data well. The use of e^+p and e^-p collision data allows, for the first time at a collider, the measurement of the beam charge asymmetry of the interference between the BH and DVCS processes. The ratio ρ of real to imaginary parts of the DVCS amplitude is then derived, directly from the measurements of the BCA and of the DVCS cross section to be $\rho = 0.20 \pm 0.05 \pm 0.08$. This ratio can also be calculated from a dispersion relation using only the DVCS energy dependence, leading to $\rho = 0.25 \pm 0.03 \pm 0.05$.

Both results are in good agreement. The GPDs model considered here [6] correctly describes the measured BCA as well as ρ. This clearly qualifies the model and its approach used for the parametrisation of GPDs. It also shows that a combined analysis of DVCS observables, including cross section and charge asymmetry, is essential for the validation of models and for the definition of their inputs.

Acknowledgements

We are grateful to the HERA machine group whose outstanding efforts have made this experiment possible. We thank the engineers and technicians for their work in constructing and maintaining the H1 detector, our funding agencies for financial support, the DESY technical staff for continual assistance and the DESY directorate for the hospitality which they extend to the non DESY members of the collaboration. We would like to thank Dieter Mueller, Kresimir Kumerički and Gregory Soyez for helpful discussions and for providing theory predictions.

References

[1] M. Diehl *et al.*, "Testing the handbag contribution to exclusive virtual Compton scattering," Phys. Lett. B **411** (1997) 193 [hep-ph/9706344].

[2] A. V. Belitsky, D. Mueller and A. Kirchner, "Theory of deeply virtual Compton scattering on the nucleon," Nucl. Phys. B **629** (2002) 323 [hep-ph/0112108].

[3] M. Burkardt, "Impact parameter space interpretation for generalized parton distributions," Int. J. Mod. Phys. A **18** (2003) 173 [hep-ph/0207047].

[4] M. Diehl, "Generalized parton distributions in impact parameter space," Eur. Phys. J. C **25** (2002) 223 [Erratum-ibid. C **31** (2003) 277] [hep-ph/0205208].

[5] L. Frankfurt, M. Strikman and C. Weiss, "Small-x physics: From HERA to LHC and beyond," Ann. Rev. Nucl. Part. Sci. **55** (2005) 403 [hep-ph/0507286].

[6] K. Kumerički, D. Mueller and K. Passek-Kumerički, "Sum rules and dualities for generalized parton distributions: Is there a holographic principle?," Eur. Phys. J. C **58** (2008) 193 [0805.0152 [hep-ph]]; 0807.0159 [hep-ph].

[7] M. Diehl *et al.*, "Generalized parton distributions from nucleon form factor data," Eur. Phys. J. C **39** (2005) 1 [hep-ph/0408173].

[8] P. Söding, Phys. Lett. **8** (1964) 285.

[9] A. Hebecker and T. Teubner, "Skewed parton distributions and F2(D) at beta $\rightarrow$ 1," Phys. Lett. B **498** (2001) 16 [hep-ph/0010273].

[10] F. D. Aaron *et al.* [H1 Collaboration], "Measurement of Deeply Virtual Compton Scattering and its t-dependence at HERA," Phys. Lett. B **659** (2008) 796 [0709.4114 [hep-ex]].

[11] M. McDermott, R. Sandapen and G. Shaw, "Colour dipoles and virtual Compton scattering," Eur. Phys. J. C **22** (2002) 655 [hep-ph/0107224].

[12] C. Marquet, R. B. Peschanski and G. Soyez, "Exclusive vector meson production at HERA from QCD with saturation," Phys. Rev. D **76** (2007) 034011 [hep-ph/0702171].

[13] C. Adloff *et al.* [H1 Collaboration], "Measurement of deeply virtual Compton scattering at HERA," Phys. Lett. B **517** (2001) 47 [hep-ex/0107005].

[14] A. Aktas *et al.* [H1 Collaboration], "Measurement of deeply virtual Compton scattering at HERA," Eur. Phys. J. C **44** (2005) 1 [hep-ex/0505061].

[15] S. Chekanov *et al.* [ZEUS Collaboration], "Measurement of deeply virtual Compton scattering at HERA," Phys. Lett. B **573** (2003) 46 [hep-ex/0305028].

[16] S. Chekanov *et al.* [ZEUS Collaboration], "A Measurement of the Q^2, W and t Dependences of Deeply Virtual Compton Scattering at HERA", submitted to JHEP, arXiv:0812.2517 [hep-ex].

[17] M. Diehl and D. Y. Ivanov, "Dispersion representations for hard exclusive processes," Eur. Phys. J. C **52** (2007) 919 [0707.0351 [hep-ph]].

[18] I. Abt *et al.* [H1 Collaboration], "The H1 detector at HERA," Nucl. Instrum. Meth. A **386** (1997) 310;
I. Abt *et al.* [H1 Collaboration], "The Tracking, calorimeter and muon detectors of the H1 experiment at HERA ," Nucl. Instrum. Meth. A **386** (1997) 348.

[19] R. D. Appuhn *et al.* [H1 SPACAL Group], Nucl. Instrum. Meth. A **386** (1997) 397.

[20] B. Andrieu *et al.* [H1 Calorimeter Group], "Beam tests and calibration of the H1 liquid argon calorimeter with electrons," Nucl. Instrum. Meth. A **350** (1994) 57.

[21] B. Roland, "Mesure de la Diffusion Compton à Haute Virtualité à HERA II", Ph.D. thesis, Université libre de Bruxelles (2007), available at http://www-h1.desy.de/psfiles/theses/.

[22] E. Perez, L. Schoeffel and L. Favart, "MILOU: A Monte-Carlo for deeply virtual Compton scattering," hep-ph/0411389.

[23] L. L. Frankfurt, A. Freund and M. Strikman, "Diffractive exclusive photoproduction in DIS at HERA," Phys. Rev. D **58** (1998) 114001 [Erratum-ibid. D **59** (1999) 119901] [hep-ph/9710356].

[24] A. Courau *et al.*, "Quasi-Real QED Compton Monte Carlo", Proceedings of the Workshop "Physics at HERA", eds. W. Buchmüller and G. Ingelman, DESY (1991), vol. 2, p. 902.

[25] B. List and A. Mastroberardino, "DIFFVM: A Monte Carlo generator for diffractive processes in ep scattering", Proceedings of the Workshop "Monte Carlo Generators for HERA Physics", eds. A. T. Doyle *et al.*, DESY (1998), p. 396.

[26] R. Brun *et al.*, "GEANT3", CERN-DD/EE/84-1.

[27] A. Aktas *et al.* [H1 Collaboration], "Elastic J/Psi production at HERA," Eur. Phys. J. C **46** (2006) 585 [hep-ex/0510016].

[28] S. Chekanov *et al.* [ZEUS Collaboration], "Exclusive electroproduction of J/Psi mesons at HERA," Nucl. Phys. B **695** (2004) 3 [hep-ex/0404008].

[29] Yu.L. Dokshitzer *et al.*, "Basics of perturbative QCD", Editions Frontières (1991), chap. 4, p107.

[30] X. Janssen, "Electroproduction diffractive de mesons Rho à HERA", Ph.D. thesis, Université libre de Bruxelles (2003), DESY-THESIS-2003-004, available at http://www-h1.desy.de/psfiles/theses/

[31] C. Adloff *et al.* [H1 Collaboration], "Proton dissociative rho and elastic Phi electroproduction at HERA," Z. Phys. C **75** (1997) 607 [hep-ex/9705014].

[32] S. Chekanov *et al.* [ZEUS Collaboration], "Exclusive electroproduction of J/psi mesons at HERA," Nucl. Phys. B **695** (2004) 3 [hep-ex/0404008].

[33] A. Airapetian *et al.* [HERMES Collaboration], "Measurement of Azimuthal Asymmetries With Respect To Both Beam Charge and Transverse Target Polarization in Exclusive Electroproduction of Real Photons," JHEP **0806** (2008) 066 [0802.2499 [hep-ex]].

[34] L. Schoeffel, "Generalised parton distributions at HERA and prospects for COMPASS," Phys. Lett. B **658** (2007) 33 [0706.3488 [hep-ph]].

[35] N. d'Hose *et al.*, "Feasibility study of deeply virtual Compton scattering using COMPASS," Nucl. Phys. A **711** (2002) 160.

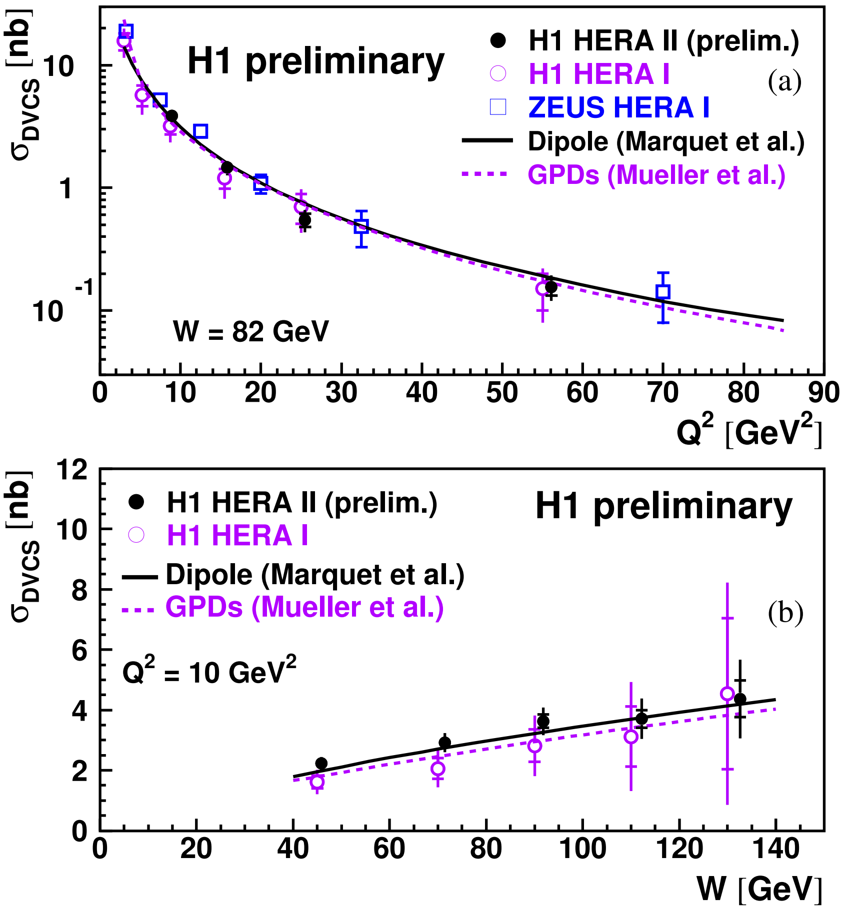

Figure 1: The DVCS cross section as a function of Q^2 at $W = 82$ GeV (a) and as a function of W at $Q^2 = 10$ GeV^2 (b). The results from the previous H1 [14] and ZEUS [16] publications based on HERA I data are also displayed. The inner error bars represent the statistical errors, the outer error bars the statistical and systematic errors added in quadrature. The dashed line represents the prediction of the GPDs model [6] and the solid line the prediction of the dipole model [12].

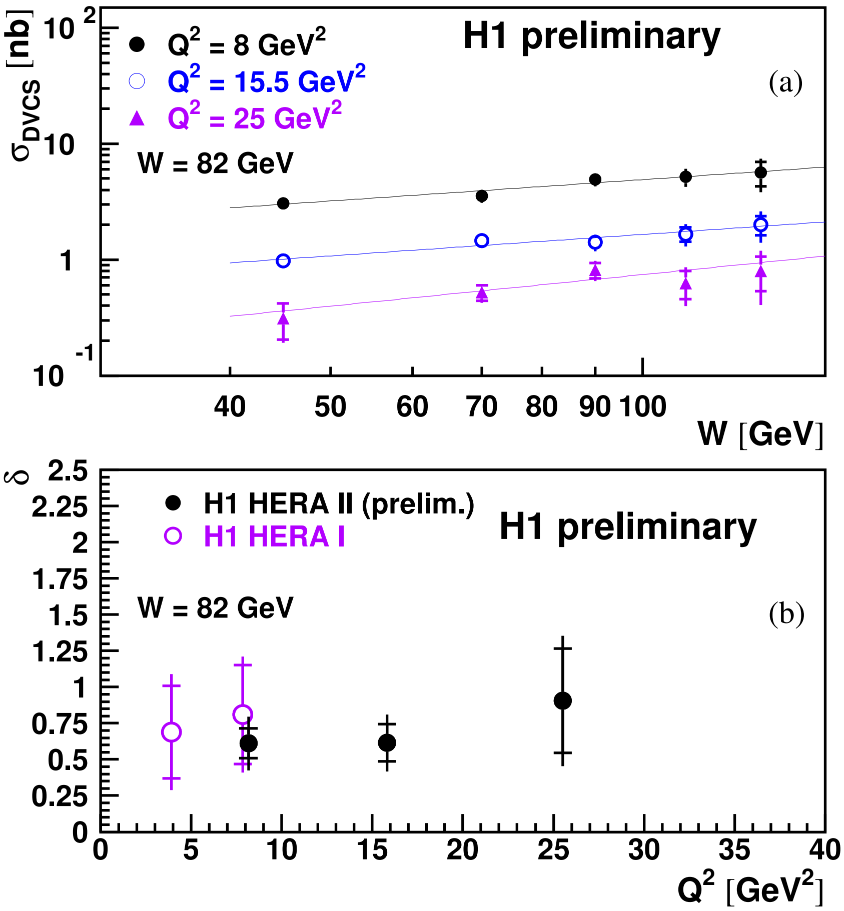

Figure 2: The DVCS cross section as a function of W at three values of Q^2 (a). The solid lines represent the results of fits of the form W^δ. The fitted values of $\delta(Q^2)$ are shown in (b) together with the values measured using HERA I data [14]. The inner error bars represent the statistical errors, the outer error bars the statistical and systematic errors added in quadrature.

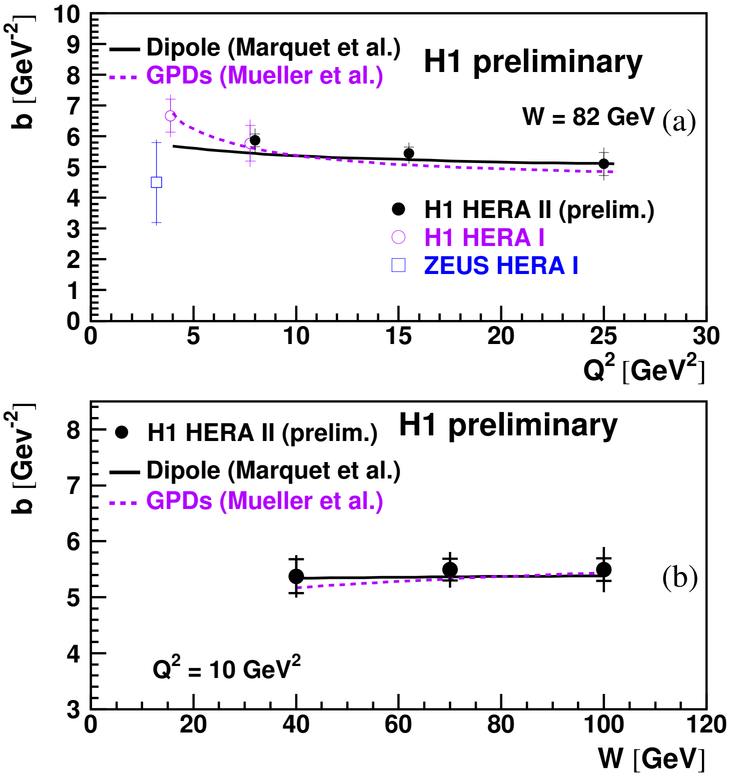

Figure 3: The fitted t–slope parameters $b(Q^2)$ are shown in (a) together with the t–slope parameters from the previous H1 [14] and ZEUS [16] publications based on HERA I data (see text). In (b) the fitted t–slope parameters $b(W)$ are shown. The inner error bars represent the statistical errors and the outer error bars the statistical and systematic errors added in quadrature. The dashed line represents the prediction of the GPDs model [6] and the solid line the prediction of the dipole model [12].

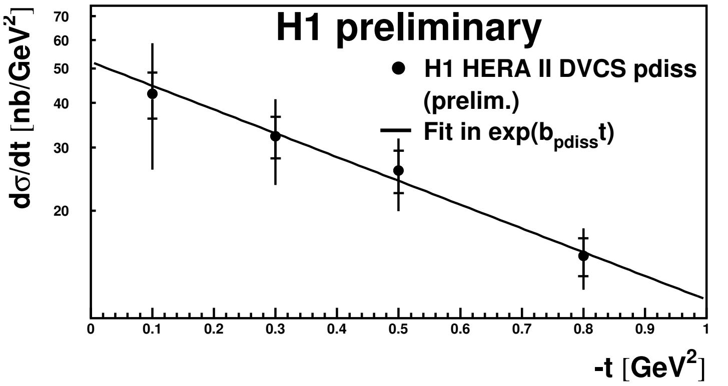

Figure 4: The inelastic DVCS cross section differential in t at $W = 82$ GeV and $Q^2 = 10\,\text{GeV}^2$. The inner error bars represent the statistical errors, the outer error bars the statistical and systematic errors added in quadrature.

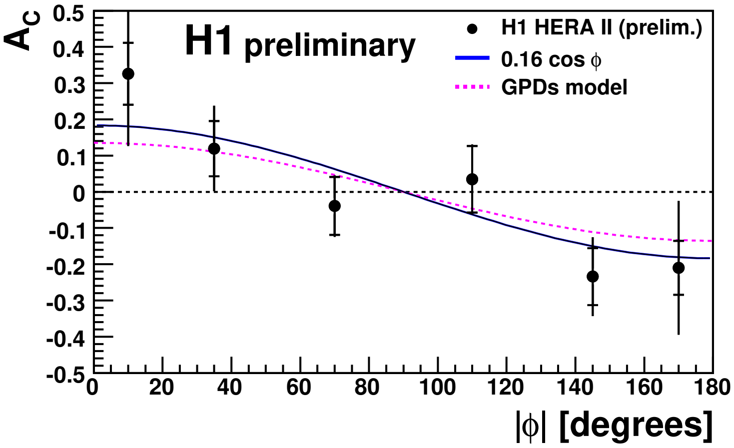

Figure 5: Beam charge asymmetry as a function of ϕ and integrated over the kinematic range of the analysis. A bin size of the order of the experimental resolution on ϕ is used. The inner error bars represent the statistical errors, the outer error bars the statistical and systematic errors added in quadrature. The function $0.16 \cos \phi$ is represented (solid line), together with the GPDs model prediction (dashed line).